

**THE SYNTHESIS OF NON-STOICHIOMETRIC CORDIERITE  
VIA GLASS CERAMIC ROUTE USING CALCINED TALC AND  
KAOLIN**

**by**

**BANJURAIZAH BT JOHAR**

**Thesis submitted in fulfillment of the requirements**

**for the degree of**

**Doctor of Philosophy**

**June 2011**

## ACKNOWLEDGEMENTS

Alhamdulillah, praised to Allah The Almighty. This thesis would never have been completed without His guidance. First and foremost I would like to express my deepest gratitude and appreciation to my main supervisor Professor Dr. Hj. Zainal Arifin Ahmad who guide and supervise my project, inspire me with advice, motivation and support. His constant enthusiasm and insightfulness will be a model for my career. Thanks to Dr. Hasmaliza Mohamad as co-supervisor. I would also like to take this opportunity to thank School of Material and Mineral Resources Engineering. Special thanks to Associate Professor Dr. Srimala Sreekantan, Professor Radzali Othman and Professor Dr. Fauziah bt Hj. Abd Aziz for giving a valuable input in the thesis. My gratitude extends to the Islamic Development Bank Saudi Arabia especially to Dato' Dr. Malek and brother Ahuq for the PhD scholarship sponsor. Grateful thanks to UNIMAP for the study leave and FRGS under grant 9003-00171 for part of research financial support. Great thanks also go to the technicians Mr. Mokhtar, Mr. Shahrul, Mr. Kemuridan, Mdm Fong, Mr. Zaini, Mr. Rashid and Mr. Azam who always be there for technical help. My time in USM would not be pleasant without the company of my friends namely Al-Amin, Hazman, Zahir, Nor Azam, Mohd Arif, Suhaina, Wanis, Nik Akmar, Wan Mohd. Fahmin, Azwadi and Norfadhilah. Lastly, my special and deepest appreciation and thanks go to my mum Hjh Zaharah and my beloved husband Hj. Mohamad Saman. Their constant support and encouragement gives the warmth and strength to me. They are always there, ever present to share my success as well as during my sad and down times. Their inspiration, understanding, patience and support help me to complete this thesis, and no words are adequate enough to express my appreciation to both of you. For my five beloved children; Nur Afiqah, Muhammad Hafizudeen, Ahmad Syamim Arsyad, Ahmad Asyraaf and Hawa, I love you all so much and you have inspired me to finish my PhD study on time.

## TABLE OF CONTENTS

<b>ACKNOWLEDGEMENTS</b>	<b>II</b>
<b>TABLE OF CONTENTS</b>	<b>III</b>
<b>LIST OF FIGURES</b>	<b>IX</b>
<b>LIST OF TABLES</b>	<b>XX</b>
<b>LIST OF ABBREVIATIONS</b>	<b>XXII</b>
<b>LIST OF SYMBOLS</b>	<b>XXIII</b>
<b>LIST OF PUBLICATIONS</b>	<b>XXVI</b>
<b>ABSTRAK</b>	<b>XXVIII</b>
<b>ABSTRACT</b>	<b>XXIX</b>
<b>CHAPTER 1 INTRODUCTION</b>	<b>1</b>
1.1 Introduction	1
1.2 Problem statement	7
1.3 Research objectives	8
1.4 Scope of research	9
<b>CHAPTER 2 LITERATURE REVIEW</b>	<b>12</b>
2.1 $\alpha$ -Cordierite	12
2.2 MgO-Al <sub>2</sub> O <sub>3</sub> -SiO <sub>2</sub> phase	12
2.3 Polymorphism of cordierite	13
2.4 Common methods for synthesis of $\alpha$ -cordierite powders	20

2.4.1 Solid state reaction	20
2.4.2 Sol-gel method	22
2.5 Crystallization of glass method	24
2.5.1 Crystallization process	25
2.5.2 Sintering aids and nucleating agent	34
2.6 Materials used for synthesis $\alpha$ -cordierite glass-ceramic	38
2.6.1 Kaolin	39
2.6.2 Talc	40
2.6.3 Alumina	40
2.6.4 Magnesia	42
2.6.5 Silica	43
2.7 $\alpha$ -Cordierite glass-ceramic process flow	44
2.7.1 Mixing	45
2.7.2 Melting and quenching	46
2.7.3 Quenching	48
2.7.4 Mechanical activation of a glass	52
2.7.5 Powder compaction/ pressing	54
2.7.6 Sintering	57
2.7.7 Crystallization of glass	62
2.8 Characterization	63
2.8.1 X-ray diffraction	63
2.8.2 Scanning Electron Microscopy (SEM)	67
2.8.3 Dielectric properties	68
2.8.4 Differential Thermal Analysis, DTA	74

2.8.5 Coefficient of thermal expansion	75
<b>CHAPTER 3 METHODOLOGY</b>	<b>79</b>
3.1 Introduction	79
3.2 Experimental design	79
3.3 General flow chart of experiment	80
3.4 Starting raw materials	81
3.5 Raw materials characterization	82
3.6 Preparation of sintered $\alpha$ -cordierite glass ceramic	82
3.6.1 Composition formulation	82
3.6.2 Mixing	88
3.6.3 Melting	89
3.6.4 Quenching	90
3.6.5 Milling	90
3.6.6 Uniaxial pressing	91
3.6.7 Sintering	92
3.7 Characterization techniques	93
3.7.1 Particle size	93
3.7.2 X-ray diffraction	94
3.7.3 Differential Thermal Analysis, DTA	97
3.7.4 Dilatometry test	98
3.7.5 Density and porosity determination	99
3.7.6 Scanning Electron Microscopy	100
3.7.7 Dielectric properties measurement	101

<b>CHAPTER 4 RESULTS AND DISCUSSIONS</b>	<b>102</b>
4.1 Results and discussions on characterization of initial raw materials used in presents research	102
4.1.1 XRD	102
4.1.2 Elemental analysis by XRF	104
4.2 Result and discussion on synthesized $\alpha$ -cordierite from various MAS ratio using mainly kaolin and talc as initial raw materials	106
4.2.1 Introduction	106
4.2.2 Characterization of glass frits and glass powders	108
4.2.3 Densification and crystallization behavior	123
4.2.4 Characterization of sintered pellet	129
4.2.5 Summary	150
4.3 Results and discussions on synthesis and characterization of $x\text{MgO}-1.5\text{Al}_2\text{O}_3-5\text{SiO}_2$ ( $x = 2.6-3$ mole) system using mainly talc and kaolin through the glass route	151
4.3.1 Introduction	151
4.3.2 Characterization of glass powder	153
4.3.3 Densification and crystallization	161
4.3.4 Characterization of sintered pellet	162
4.3.5 Summary	175
4.4 Effect of fixed amount of $\text{B}_2\text{O}_3$ and $\text{P}_2\text{O}_5$ addition in various MAS compositions using mainly talc and kaolin as initial raw materials.	176
4.4.1 Introduction	176

4.4.2 Characterization of glass powder	179
4.4.3 Densification and crystallization behavior	195
4.4.4 Characterization of sintered pellet	196
4.4.5 Summary	223
4.5 Results and discussions on synthesize and characterization of various MAS ratio using pure oxides as initial raw materials	224
4.5.1 Introduction	224
4.5.2 Characterization of glass powder	225
4.5.3 Densification and crystallization	236
4.5.4 Characterization of sintered pellet	237
4.5.5 Summary	252
4.6 Results and discussions on comparative study on the densification, crystallization and properties of samples synthesized using pure oxides and minerals	253
4.6.1 Introduction	253
4.6.2 Characterization of glass frits and glass powder	254
4.6.3 Densification and crystallization behavior	260
4.6.4 Characterization of sintered pellet	261
4.6.5 Summary	270
4.7 Results and discussions on the effect of melting temperature on the densification, crystallization and properties of single phase and low sintering temperature of $\alpha$ -cordierite.	271
4.7.1 Introduction	271
4.7.2 Characterization of glass powder	272

4.7.3	Densification and crystallization	282
4.7.4	Characterization of sintered pellet	283
4.7.5	Summary	296
<b>CHAPTER 5 CONCLUSIONS</b>		<b>298</b>
5.1	Conclusions	298
5.2	Future work	304



## LIST OF FIGURES

		Page
Figure 2.1	Ternary phase diagram of MgO-Al <sub>2</sub> O <sub>3</sub> -SiO <sub>2</sub> [42]	13
Figure 2.2	Diffraction pattern and crystal structure plots of $\mu$ -cordierite and $\beta$ -quartz	14
Figure 2.3	Crystal structure of $\alpha$ -cordierite (ICSD 98-004-1938)	15
Figure 2.4	Crystal structure of $\beta$ -cordierite (ICSD 98-010-9834)	15
Figure 2.5	Crystal structure of $\mu$ -cordierite (ICSD 98-001-3453)	16
Figure 2.6	Reference pattern of 3 cordierite polymorphs $\alpha$ -cordierite, $\beta$ -cordierite, $\mu$ -cordierite	17
Figure 2.7	Diffraction pattern of hexagonal and orthorhombic cordierite can be distinguished after zooming at 2 Theta 28-30°	18
Figure 2.8	Al-Si ordering sequence in $\beta$ -cordierite	19
Figure 2.9	Critical radius of nuclei formation versus the change in free energy, $\Delta G$ [55]	28
Figure 2.10	Two phase separation of glass	35
Figure 2.11	$\alpha$ -Cordierite glass-ceramic process flow	45
Figure 2.12	Time-Temperature-Transformation (TTT) curves representing supercooled melts with low (curve A) and high viscosity (curve B) at $T_m$ . The dashed lines represent the critical cooling rates to avoid crystallization [70, 71]	49
Figure 2.13	Volume-temperature relationship for glasses, liquids, supercooled liquids and crystal. [72]	51
Figure 2.14	Pressure gradient within the powders in a die cavity when uni-axially pressed from above [66]	56
Figure 2.15	Schematic representation of the sintering and crystallization process of the glass having cordierite composition [78].	61
Figure 2.16	Schematic representation of four polarization	

	mechanisms	71
Figure 2.17	Frequency dependency of polarizability	74
Figure 2.18	Inter-atomic potential [89]	77
Figure 3.1	Flow chart of experiment	80
Figure 3.2	General profile temperature for glass melting	89
Figure 3.3	Temperature profile for sintering	93
Figure 3.4	Non-isothermal and isothermal DTA temperature profile	98
Figure 4.1	Diffraction pattern of kaolin powder, (K; kaolin ICSD 98-005-2652, M: muscovite ICSD 98-009-8687, Q: quartz ICSD 98-010-7204)	103
Figure 4.2	Diffraction pattern of talc powder. T: talc, ICSD 98-001-2209, m: magnesite: ICSD 98-002-1925, D: dolomite ICSD 98-009-4816,Q: quartz ICSD 98-010-7204	103
Figure 4.3	Diffraction pattern of magnesia powder, magnesia: ICSD 98-005-3326	104
Figure 4.4	Diffraction pattern of alumina powder, (c: corundum, Al <sub>2</sub> O <sub>3</sub> ICSD 98-006-7021)	105
Figure 4.5	Diffraction pattern of silica powder, (Q: quartz ICSD 98-010-7204)	105
Figure 4.6	Photograph of glass frits, a): sample A1, b): sample A2, c): sample A3, d): sample A4, e): sample A5, f): sample A6, g): sample A7	108
Figure 4.7	Density distributions of various glass powder samples as a function of particle size	109
Figure 4.8	Morphology of glass powders samples; a) sample A1, b) sample A2, c) sample A3, d) sample A4, e) sample A5, f) sample A6, and g) sample A7	111
Figure 4.9	X-ray diffraction patterns of glass powder with various MgO:Al <sub>2</sub> O <sub>3</sub> :SiO <sub>2</sub> ratio; s: spinel, M: mullite, WC:tungsten carbide, Q-quartz	112
Figure 4.10	Non-isothermal DTA curves with various compositions	114

Figure 4.11	Crystallization temperature of samples with various MgO mole	115
Figure 4.12	DTA curves with isothermal heating at 900°C for 2 h	116
Figure 4.13	Dilatometric curve of green compacted glass with various compositions. a) The whole profile dilatometry curves, b) Dilatometry curves zoom at shrinkage area.	118
Figure 4.14	Microstructure of pressed pellet samples heated at non-isothermal temperature; a) A4 sample heated at 825°C, b) A4 sample heated at 930°C, c) A6 sample heated at 825°C, and d) A6 sample heated at 930°C	120
Figure 4.15	Arrhenius plot to determine activation energy for densification.	123
Figure 4.16	Densification and crystallization temperature of samples with excess MgO mole	125
Figure 4.17	Microstructure of fracture surface sintered isothermally at 900°C for 15 min; a) sample A4, and b) sample A6	126
Figure 4.18	Microstructure of sample A4 sintered at 900°C for 2 h; a) fracture surface, and b) etched surface	126
Figure 4.19	Percent shrinkage in samples with increasing MgO	128
Figure 4.20	X-ray diffraction pattern of heat treated samples with excess MgO mole; m:mullite, $\alpha$ : $\alpha$ -cordierite, s:spinel, $\mu$ : $\mu$ -cordierite, and F:forsterite.	131
Figure 4.21	Example of Rietveld plots; a) sample A1 (2MgO.2Al <sub>2</sub> O <sub>3</sub> .5SiO <sub>2</sub> , and b) sample A4 (2.8MgO.2Al <sub>2</sub> O <sub>3</sub> .5SiO <sub>2</sub> )	134
Figure 4.22	Comparison between plots of intensity and weight percent of phase versus MgO mol ratio for all phases a) $\alpha$ -cordierite, b) spinel c) forsterite, and d) $\mu$ -cordierite	137
Figure 4.23	Count of intensity of $\alpha$ -cordierite peak (taken at five different planes) as a function of MgO mole ratio.	138
Figure 4.24	Changes of lattice a and lattice c as a function of MgO mole	139
Figure 4.25	Density and porosity of samples with increasing MgO mole	140

Figure 4.26	Microstructure of fracture surface (A1 to A7) sintered at 900°C for 2 h	142
Figure 4.27	Thermal expansion coefficient with increasing MgO mole	143
Figure 4.28	Dielectric constant of samples as a function of frequency	146
Figure 4.29	Dielectric constant of sintered samples as a function of MgO mole measured at 1 GHz	146
Figure 4.30	Dielectric loss of sample as a function of frequency	149
Figure 4.31	Dielectric loss as a function of MgO mole	149
Figure 4.32	Morphology of glass powders samples in $x\text{MgO}.1.5\text{Al}_2\text{O}_3.5\text{SiO}_2$ series; a) sample A8 (3:1.5:5), b) sample A9 (2.8:1.5:5), and c) sample A10 (2.6:1.5:5)	153
Figure 4.33	XRD patterns of glass powder for sample sample A8, A9 and A10	154
Figure 4.34	DTA curves of samples with various MAS ratio	155
Figure 4.35	Crystallization temperatures of samples with increasing MgO mole for series $x\text{MgO}.1.5\text{Al}_2\text{O}_3.5\text{SiO}_2$ .	156
Figure 4.36	Integrated area under DTA peak.	157
Figure 4.37	Isothermal DTA plot for sample A8, A9 and A10	158
Figure 4.38	Dilatometry curves of MAS glass powder samples ( $x\text{MgO}.1.5\text{Al}_2\text{O}_3.5\text{SiO}_2$ )	159
Figure 4.39	Activation energy for densification of glass powder samples with compositions $x\text{MgO}.1.5\text{Al}_2\text{O}_3.5\text{SiO}_2$ .	160
Figure 4.40	Densification and crystallization temperature of samples vs MgO mole	161
Figure 4.41	X-ray diffraction pattern of samples with different MAS ratio sintered at 900°C for 2 h; $\alpha$ : $\alpha$ -cordierite, $\mu$ : $\mu$ -cordierite, F: forsterite, and Sp: spinel	163
Figure 4.42	The intensity of $\alpha$ -cordierite peak count at (022) plane as a function of MgO mole	164

Figure 4.43	Rietveld Plot of sample A10 (2.6:1.5:5)	165
Figure 4.44	Lattice changes as a function of MgO mole; a) Lattice- <i>a</i> , b) Lattice- <i>c</i>	167
Figure 4.45	Bulk density and porosity percentage of samples vs MgO in series of $x\text{MgO}.1.5\text{Al}_2\text{O}_3.5\text{SiO}_2$ mole ratio.	168
Figure 4.46	Microstructure of fracture surface of sample a) A8 (3:1.5:5), b) A9(2.8:1.5:5), and c) A10 (2.6:1.5:5) sintered at 900°C for 2 h	169
Figure 4.47	Dielectric constant in series of $x\text{MgO}.1.5\text{Al}_2\text{O}_3.5\text{SiO}_2$ samples as a function of frequency	171
Figure 4.48	Dielectric constant of samples with different MAS ratio for sample A8, A9, and A10	172
Figure 4.49	Dielectric loss of samples as a function of frequency	173
Figure 4.50	Dielectric loss of samples at 1 GHz as a function of MgO mole	173
Figure 4.51	Proportion line for calculating coefficient of thermal expansion of sintered rectangular pellet of sample A8, A9 and A10	174
Figure 4.52	Coefficient of thermal expansion of samples A8, A9 and A10	175
Figure 4.53	Distribution of particle size for various glass powders composition	179
Figure 4.54	Morphology of glass powder samples with $\text{B}_2\text{O}_3$ and $\text{P}_2\text{O}_5$ (s); a) sample A1s, b) sample A2s, c) sample A4s, d) sample A5s, e) sample A8s, f) sample A9s, and g) sample A10s	180
Figure 4.55	Diffraction pattern of glass powder with various MAS ratio that contain $\text{B}_2\text{O}_3$ and $\text{P}_2\text{O}_5$ ; a) series of $x\text{MgO}.2\text{Al}_2\text{O}_3.5\text{SiO}_2 + \text{B}_2\text{O}_3$ and $\text{P}_2\text{O}_5$ , and b) series of $x\text{MgO}.1.5\text{Al}_2\text{O}_3.5\text{SiO}_2 + \text{B}_2\text{O}_3$ and $\text{P}_2\text{O}_5$ . (m: mullite)	182
Figure 4.56	Comparison on the diffraction pattern of glass powder for series of samples with and without $\text{B}_2\text{O}_3$ and $\text{P}_2\text{O}_5$ . * s represents sample with $\text{B}_2\text{O}_3$ and $\text{P}_2\text{O}_5$	183
Figure 4.57	Crystallization peak of samples with different MAS ratio; a) series of $x\text{MgO}.2\text{Al}_2\text{O}_3.5\text{SiO}_2 + \text{B}_2\text{O}_3$ and $\text{P}_2\text{O}_5$	

	, and b) series of $x\text{MgO} \cdot 1.5\text{Al}_2\text{O}_3 \cdot 5\text{SiO}_2 + \text{B}_2\text{O}_3$ and $\text{P}_2\text{O}_5$ .	184
Figure 4.58	DTA curves comparison between glass sample with and without $\text{B}_2\text{O}_3$ and $\text{P}_2\text{O}_5$ for series $x\text{MgO} \cdot 2\text{Al}_2\text{O}_3 \cdot 5\text{SiO}_2$	186
Figure 4.59	DTA curves comparison between glass sample with and without $\text{B}_2\text{O}_3$ and $\text{P}_2\text{O}_5$ for series $x\text{MgO} \cdot 1.5\text{Al}_2\text{O}_3 \cdot 5\text{SiO}_2$	187
Figure 4.60	Comparison on crystallization temperature ( $T_p$ ) between sample with and without $\text{B}_2\text{O}_3$ and $\text{P}_2\text{O}_5$ ; a) samples in series $x\text{MgO} \cdot 2\text{Al}_2\text{O}_3 \cdot 5\text{SiO}_2 + \text{B}_2\text{O}_3$ and $\text{P}_2\text{O}_5$ , and b) samples in series $x\text{MgO} \cdot 1.5\text{Al}_2\text{O}_3 \cdot 5\text{SiO}_2 + \text{B}_2\text{O}_3$ and $\text{P}_2\text{O}_5$ )	189
Figure 4.61	Comparison on the area under DTA peak between sample with and without $\text{B}_2\text{O}_3$ and $\text{P}_2\text{O}_5$ ; a) sample in series $x\text{MgO} \cdot 2\text{Al}_2\text{O}_3 \cdot 5\text{SiO}_2 + \text{B}_2\text{O}_3$ and $\text{P}_2\text{O}_5$ , and b) sample in series $x\text{MgO} \cdot 1.5\text{Al}_2\text{O}_3 \cdot 5\text{SiO}_2 + \text{B}_2\text{O}_3$ and $\text{P}_2\text{O}_5$	190
Figure 4.62	Dilatometry plots of compact glass powder samples heated non-isothermally from room temperature to elevated temperature.	191
Figure 4.63	Comparison on dilatometry curve of glass powder between samples with and without $\text{B}_2\text{O}_3$ and $\text{P}_2\text{O}_5$ .	193
Figure 4.64	Activation energy for densification for glass powder samples with the addition of $\text{B}_2\text{O}_3$ and $\text{P}_2\text{O}_5$ .	195
Figure 4.65	Densification and crystallization of glass sample with the addition of $\text{B}_2\text{O}_3$ and $\text{P}_2\text{O}_5$	196
Figure 4.66	Diffraction pattern of sintered pellet with $\text{B}_2\text{O}_3$ and $\text{P}_2\text{O}_5$ ; a) series of $x\text{MgO} \cdot 2\text{Al}_2\text{O}_3 \cdot 5\text{SiO}_2$ , and b) series of $x\text{MgO} \cdot 1.5\text{Al}_2\text{O}_3 \cdot 5\text{SiO}_2$ .	198
Figure 4.67	Comparisons on count of intensity of $\alpha$ -cordierite between samples with and without $\text{B}_2\text{O}_3$ and $\text{P}_2\text{O}_5$ as a function of MgO; a) series $x\text{MgO} \cdot 2\text{Al}_2\text{O}_3 \cdot 5\text{SiO}_2$ and b) series $x\text{MgO} \cdot 1.5\text{Al}_2\text{O}_3 \cdot 5\text{SiO}_2$	201
Figure 4.68	Effect of MgO (mole) to degree of crystallinity; a) series of $x\text{MgO} \cdot 2\text{Al}_2\text{O}_3 \cdot 5\text{SiO}_2 + \text{B}_2\text{O}_3$ and $\text{P}_2\text{O}_5$ , and b) series of $x\text{MgO} \cdot 1.5\text{Al}_2\text{O}_3 \cdot 5\text{SiO}_2 + \text{B}_2\text{O}_3$ and $\text{P}_2\text{O}_5$ .	203

Figure 4.69	Percent and peak area of alpha cordierite as a function of MgO a) series of $x\text{MgO}.2\text{Al}_2\text{O}_3.5\text{SiO}_2 + \text{B}_2\text{O}_3$ and $\text{P}_2\text{O}_5$ , and b) series of $x\text{MgO}.1.5\text{Al}_2\text{O}_3.5\text{SiO}_2 + \text{B}_2\text{O}_3$ and $\text{P}_2\text{O}_5$ .	207
Figure 4.70	Lattice parameter for sample with various compositions; a) series of $x\text{MgO}.2\text{Al}_2\text{O}_3.5\text{SiO}_2 + \text{B}_2\text{O}_3$ and $\text{P}_2\text{O}_5$ , and b) series of $x\text{MgO}.1.5\text{Al}_2\text{O}_3.5\text{SiO}_2 + \text{B}_2\text{O}_3$ and $\text{P}_2\text{O}_5$ .	209
Figure 4.71	Bulk density of heat treatment of compacted glass pellet with $\text{B}_2\text{O}_3$ and $\text{P}_2\text{O}_5$ as a function of MgO mole; a) series $x\text{MgO}.2\text{Al}_2\text{O}_3.5\text{SiO}_2$ , and b) series $x\text{MgO}.1.5\text{Al}_2\text{O}_3.5\text{SiO}_2$	210
Figure 4.72	Percent porosity of heat treatment compacted glass sample as a function of MgO mole; a) series $x\text{MgO}.2\text{Al}_2\text{O}_3.5\text{SiO}_2$ , and b) series $x\text{MgO}.1.5\text{Al}_2\text{O}_3.5\text{SiO}_2$	211
Figure 4.73	Shrinkage percentage of sintered pellet samples with $\text{B}_2\text{O}_3$ and $\text{P}_2\text{O}_5$ ;	211
Figure 4.74	The FESEM micrograph of fracture surface of glass ceramic with $\text{B}_2\text{O}_3$ and $\text{P}_2\text{O}_5$ ; a) A1s, b) A2s, c) A4s, and d) A5s	212
Figure 4.75	The FESEM micrograph of fracture surface of glass ceramic with $\text{B}_2\text{O}_3$ and $\text{P}_2\text{O}_5$ ; a) A8s, b) A9s, and c) A10s	213
Figure 4.76	Dielectric constant of samples with various MAS ratio at frequency 1 MHz to 1.8 GHz for sintered samples with $\text{B}_2\text{O}_3$ and $\text{P}_2\text{O}_5$ ; a) series of $x\text{MgO}.2\text{Al}_2\text{O}_3.5\text{SiO}_2$ samples and b) series of $x\text{MgO}.1.5\text{Al}_2\text{O}_3.5\text{SiO}_2$ samples	214
Figure 4.77	Comparison on the dielectric constant of heat treated samples at 1 GHz with and without $\text{B}_2\text{O}_3$ and $\text{P}_2\text{O}_5$ as a function of MgO mole; a) trend for samples in series $x\text{MgO}.2\text{Al}_2\text{O}_3.5\text{SiO}_2$ samples, and b) trend after result of sample A2s was removed	216
Figure 4.78	Comparison on dielectric constant of heat treated samples at 1 GHz with and without $\text{B}_2\text{O}_3$ and $\text{P}_2\text{O}_5$ as a function of MgO mole in series of $x\text{MgO}.1.5\text{Al}_2\text{O}_3.5\text{SiO}_2$ samples with and without $\text{B}_2\text{O}_3$ and $\text{P}_2\text{O}_5$	217

Figure 4.79	Dielectric loss of samples with $B_2O_3$ and $P_2O_5$ at various frequency; a) series of $xMgO.2Al_2O_3.5SiO_2$ samples, and b) series of $xMgO.1.5Al_2O_3.5SiO_2$ samples	218
Figure 4.80	Comparison between sample with and without $B_2O_3$ and $P_2O_5$ in two series of samples a) series of $xMgO.2Al_2O_3.5SiO_2$ samples, and b) series of $xMgO.1.5Al_2O_3.5SiO_2$ samples	220
Figure 4.81	Effect of MgO mole to CTE for sample with and without $B_2O_3$ and $P_2O_5$ at frequency 1 GHz; a) series of $xMgO.2Al_2O_3.5SiO_2$ samples, and b) series of $xMgO.1.5Al_2O_3.5SiO_2$ samples.	222
Figure 4.82	Photograph of glass frits produced from pure oxides; a) sample P1s, b) sample P4, c) sample P7, d) sample P8s, and e) sample P9.	226
Figure 4.83	Morphology of glass powder for series of pure oxide samples; a) P1s, b) P4, c) P7, and d) P8s	227
Figure 4.84	X-ray diffraction pattern of fine glass powder for series of pure oxides samples; m: mullite	228
Figure 4.85	Non-isothermal Differential Thermal Analysis plots of various MAS glass powder synthesize using pure oxides.	231
Figure 4.86	Crystallization temperature (onset, peak and finished) of various pure oxide samples measured from exothermal peak in non-isothermal curve.	232
Figure 4.87	Calculated area under exothermal DTA peaks of oxide samples with different MAS ratio	234
Figure 4.88	Dilatometry curves of green pellets with various MAS ratio heated non-isothermally from room temperature to $1000^\circ C$	235
Figure 4.89	Activation energy for densification for samples with different compositions	236
Figure 4.90	Densification and crystallization temperature of pure oxide samples	237
Figure 4.91	X-ray diffraction pattern of heat treated samples synthesized using pure oxides as initial raw materials.	238



Figure 4.92	Intensity counts at various planes for sintered pure oxides samples	240
Figure 4.93	Changes of Lattice <i>a</i> and Lattice <i>c</i> of $\alpha$ -cordierite phase with compositions using pure oxide samples	243
Figure 4.94	Shrinkage percentage of pure oxides samples measured in sintered pellet	244
Figure 4.95	Bulk density of sintered pure oxide samples with different compositions	245
Figure 4.96	Percent of porosity on sintered pure oxide samples.	245
Figure 4.97	Microstructure of fracture sample for series of pure oxide samples with various MAS ratio; a) P1s, b) P4, c) P7, d) P8s, and e) P9	246
Figure 4.98	CTE of samples with different MAS ratio synthesized using pure oxides.	247
Figure 4.99	Dielectric constant of pure oxides samples with different MAS ratio.	249
Figure 4.100	Dielectric constant of pure metal oxides sample with different MAS ratio at 1 GHz frequency	249
Figure 4.101	Dielectric loss of pure oxide samples with various MAS ratio measured at 1 MHz to 1.8 GHz)	250
Figure 4.102	Dielectric loss of pure oxide samples at frequency 1 GHz	251
Figure 4.103	Picture of frits for non-stoichiometric cordierite ( $2.8\text{MgO}.1.5\text{Al}_2\text{O}_3.5\text{SiO}_2$ ) samples with different initial raw materials: a) pure oxide, and b) mineral	254
Figure 4.104	X-ray diffraction pattern of milled glass powder of sample with formulation $2.8\text{MgO}.1.5\text{Al}_2\text{O}_3.5\text{SiO}_2$ , sample A: synthesized from minerals; sample P: synthesized from pure oxides	256
Figure 4.105	Non-isothermal DTA analysis of samples with different initial raw materials; sample A-mineral, and sample P-pure oxide	257
Figure 4.106	Dilatometry curves of green rectangular pellets for both samples synthesized from pure oxides and minerals at 5 K/min from 32°C to temperature at which	

	the densification stop or shrinkage plateau.	259
Figure 4.107	Densification and crystallization temperature	260
Figure 4.108	Comparison on X-ray diffraction pattern of sintered pellet between samples synthesized from pure oxides and minerals ( $\alpha$ : $\alpha$ -cordierite, $\mu$ : $\mu$ -cordierite)	262
Figure 4.109	Diffraction pattern of both sintered sample zoom in 2 Theta 18.8° to 30°	262
Figure 4.110	Microstructure of etched surface; a) sample A, and b) sample P	266
Figure 4.111	Microstructure of fracture surface; a) sample A, and b) sample P	267
Figure 4.112	Comparison on dielectric constant of pure oxide and mineral sample as a function of frequency.	268
Figure 4.113	Comparison on dielectric loss between pure oxide and minerals samples as a function of frequency	269
Figure 4.114	Photograph of glass frits melting at different temperature;	272
Figure 4.115	Distribution of glass particles synthesized at different melting temperature 1350, 1385, 1400, 1425 and 1500°C	274
Figure 4.116	Morphology of glass powder samples melting at different temperature, a) 1500°C, b) 1425°C, c) 1400°C, d) 1385°C and e) 1350°C	275
Figure 4.117	Diffraction pattern of glass powder for samples melted at various temperatures (1350, 1385, 1400, 1425 and 1500°C); $\alpha$ : $\alpha$ -cordierite, Sp: spinel	276
Figure 4.118	Percent of amorphous content in fine glass powder as a function of melting temperature determined by FullProfile method.	277
Figure 4.119	DTA curves of sample melted at 1350, 1385, 1400, 1425 and 1500°C	279
Figure 4.120	Area under exothermic peaks for samples melted at different temperature	280
Figure 4.121	Dilatometry curves of 2.8MgO.1.5Al <sub>2</sub> O <sub>3</sub> .5SiO <sub>2</sub>	

	compacted glass which was melted at different melting temperature.	281
Figure 4.122	Effect of melting temperature to Activation energy for densification of the glass-ceramic.	282
Figure 4.123	Effect of melting temperature on densification and crystallization of $2.8\text{MgO}1.5\text{Al}_2\text{O}_3.5\text{SiO}_2$ . $T_o$ (crys): Temperature at which crystallization start, $T_f$ (crys): temperature at which crystallization end, $T_o$ (dens): temperature at which densification start, $T_f$ (dens): temperature at which densification stopped	283
Figure 4.124	X-ray Diffraction pattern for sintered samples melted at 1350, 1385, 1400, 1425 and 1500°C. a) Two theta position at 10°-30°, b) Two theta position at 30°-60°, and c) Two theta position at 60°-90° ( $\alpha$ : $\alpha$ -cordierite, sp: spinel, Q: quartz)	285
Figure 4.125	Effect of melting temperature to Intensity of $\alpha$ -cordierite phase measured at 3 strongest peak of $\alpha$ -cordierite	286
Figure 4.126	Degree of crystallinity of $\alpha$ -cordierite phase as a function of temperature of melting.	287
Figure 4.127	Weight percent of $\alpha$ -cordierite from total crystalline phase as a function of temperature of melting	289
Figure 4.128	Bulk density of samples melted at different melting temperature	290
Figure 4.129	Percent of porosity in samples melted at different melting temperature	291
Figure 4.130	Microstructure of fracture sample melted at various melting temperature; a) 1350°C, b) 1385°C, c) 1400°C, d) 1425°C, e) 1500°C	292
Figure 4.131	Dielectric constant of all samples as a function of frequency	293
Figure 4.132	Effect of melting temperature on dielectric constant measured at frequency 1 GHz	294
Figure 4.133	Dielectric loss as a function of frequency	295
Figure 4.134	Effect of melting temperature to dielectric loss of $2.8\text{MgO}1.5\text{Al}_2\text{O}_3.5\text{SiO}_2$ glass ceramic	296

## LIST OF TABLES

		<b>Page</b>
Table 2.1	Crystal data for $\mu$ -cordierite, $\alpha$ -cordierite and $\beta$ -cordierite taken from Inorganic Crystal Structure Database (ICSD)	16
Table 2.2	Sintering mechanisms in polycrystalline and amorphous solids [73]	60
Table 3.1	Oxides compositions of samples with $x\text{MgO}.2\text{Al}_2\text{O}_3.5\text{SiO}_2$ series.	84
Table 3.2	Composition of initial powders in $x\text{MgO}.2\text{Al}_2\text{O}_3.5\text{SiO}_2$ sample	84
Table 3.3	Oxides compositions of samples with $x\text{MgO}.1.5\text{Al}_2\text{O}_3.5\text{SiO}_2$ series.	85
Table 3.4	Composition of initial powders in $x\text{MgO}.1.5\text{Al}_2\text{O}_3.5\text{SiO}_2$ samples	85
Table 3.5	Oxides compositions of samples with fixed amount of sintering aids	86
Table 3.6	Composition of initial powder in mineral samples with the addition of fixed amount of sintering aids	87
Table 3.7	Compositions of initial raw material for glass ceramic synthesize using pure oxides	87
Table 3.8	Composition (wt%) of initial raw materials for both samples (pure oxide and minerals) with formulation $2.8\text{MgO}.1.5\text{Al}_2\text{O}_3.5\text{SiO}_2$	88
Table 4.1	Elementals analysis of minerals by XRF	106
Table 4.2	Average of particle size measured by Hellos	110
Table 4.3	Quantitative phase analysis of glass powder samples	113
Table 4.4	Shrinkage percentage in sintered cylindrical pellets after the non-isothermal heating	119
Table 4.5	Results of activation energy and thermal expansion coefficient of compact glass sample	123

Table 4.6	Compositions of phases present in the heat treated samples	135
Table 4.7	Results of Rietveld refinement	166
Table 4.8	Crystallization temperature of samples with B <sub>2</sub> O <sub>3</sub> and P <sub>2</sub> O <sub>5</sub> .	185
Table 4.9	Intensity of $\alpha$ -cordierite phase at selected planes.	200
Table 4.10	Rietveld quantitative phase analysis on sintered sample	205
Table 4.11	Phase analysis of sintered samples with amorphous quantification	206
Table 4.12	Coefficient of thermal expansion of sintered samples	221
Table 4.13	Quantitative phase analysis of glass powder samples synthesized from pure oxides.	229
Table 4.14	Results of Rietveld quantitative phase analysis for sintered pure oxide samples	242
Table 4.15	Activation energy for densification for pure oxide and mineral glass with composition 2.8MgO.1.5Al <sub>2</sub> O <sub>3</sub> .5SiO <sub>2</sub>	260
Table 4.16	Quantitative phase analysis of heat treated sample synthesis from pure oxide and mineral precursor of the same MAS ratio.	263
Table 4.17	Comparison on crystal structure of $\alpha$ -cordierite phase in sample synthesized from pure oxide and minerals.	264
Table 4.18	Bulk density, percent of porosity and shrinkage of sintered sample	265
Table 4.19	Coefficient of thermal expansion of sintered pellet	270
Table 4.20	Quantitative analysis of glass powder melted at different temperature.	277
Table 4.21	Crystallization temperature of samples 2.8MgO.1.5Al <sub>2</sub> O <sub>3</sub> .5SiO <sub>2</sub> glass-ceramic melted at different temperature of melting	280
Table 4.22	Results of Rietveld refinement on 2.8MgO.2Al <sub>2</sub> O <sub>3</sub> .5SiO <sub>2</sub> sintered samples melted at different temperature	288

## LIST OF ABBREVIATIONS

IC	-	Integrated circuit
DTA	-	Differential Thermal Analyses
XRF	-	X-ray florescence
XRD	-	X-ray diffraction
FEG	-	Field emission gun
BSE	-	Backscattered electron
SEI	-	Secondary electron Image
PSD	-	Particle size distribution
HELOS	-	Helium neon optical system
CTE	-	Coefficient of thermal expansion
MAS	-	Magnesium aluminum silicate
APS	-	Amorphous phase separation
ICSD	-	Inorganic Crystal Structure Data
ICDD	-	Inorganic Crystalline Diffraction Data
PDF	-	Powder diffraction file
TEOS	-	Tetraethylorthosilicate
SRM	-	Standard reference material
NIST	-	National institute of standard technologist
RIR	-	Reference intensity ratio
wt%	-	Weight percent
kJ	-	Kilo joule
rpm	-	Rotation per minute
μm	-	Micron meter
MPa	-	Mega Pascal

## LIST OF SYMBOLS

$\alpha'$	:	Total polarization
$\alpha_e$	:	Electronic polarization
$\alpha_i$	:	Ionic polarization
$\alpha_o$	:	Orientation polarization
$\alpha_f$	:	Interfacial polarization
$\alpha''$	:	Polarizability of each molecule
$\sigma'$	:	Thermal stress
$\sigma_i$	:	Interfacial energy
$\alpha_l$	:	Linear thermal expansion
$\alpha_a$	:	CTE at lattice $a$ direction
$\Delta$	:	Distortion index
$D$	:	Diffusion coefficient
$d$	:	Inter planar spacing
$E$	:	Elastic modulus
$\varepsilon$	:	Relative dielectric constant
$\varepsilon''$	:	Loss factor
$\varepsilon_o$	:	Permittivity of free space
$I_o$	:	Nucleation rate
$U$	:	Crystal growth rate
$\Delta G$	:	Gibbs free energy
$\Delta G_D$	:	Diffusion rate
$\eta$	:	Viscosity coefficient
$H$	:	Entalphy
$\rho$	:	Density
$\Delta E$	:	Energy barrier or activation energy
$a$	:	Inter atomic spacing
$v$	:	Atomic jump frequency
$c$	:	Constant
$c'$	:	Concentration
$\sigma$	:	Conductivity
$F$	:	Frequency

$F_o$	:	Resonance frequency
$\gamma$	:	Surface tension
$I_o$	:	Observed diffraction line
$I_c$	:	Calculated diffraction line
$l_i$	:	Initial length at room temperature
$l_f$	:	Length at final temperature
$J$	:	Flux
$k$	:	Dielectric constant
$M_e$	:	Mass of electron
$M$	:	Metal species
$m$	:	Slope in Arrhenius plot
$\eta$	:	Wavelength
$n$	:	Integer
OR	:	Alkoxy group
$P_n$	:	Pressure at n area
$Q$	:	Activation energy for densification
$\Theta$	:	Theta
$R$	:	Gas constant
$R_{Bragg}$	:	Agreement indice on Bragg value
$R_{wp}$	:	Agreement indices on weighted value
$R_{exp}$	:	Agreement indexed on expected value
$R_p$	:	Agreement indices on profile value
$r^*$	:	Critical radius
$S$	:	Entropy
$s$	:	Goodness of fit
$T_g$	:	Glass transition temperature
$t_n$	:	Minimum quenching time to avoid crystallization
$\tan \alpha$	:	Dissipation factor
$T_p$	:	Crystallization temperature at peak in exothermal DTA curve
$T_i$	:	Initial temperature
$T_f$	:	Final temperature
$T_m$	:	Melting temperature
$V$	:	Volume



$V_i$	:	Volume fraction of each phase
$\nu$	:	Poisson ratio
$W^*$	:	Thermodynamic barrier
$W_d$	:	Weight of dry pellet
$W_s$	:	Weight of suspended pellet
$W_w$	:	Weight of saturated pellet
$X_c$	:	Crystallization mass fraction
$X_a$	:	Non-crystallized mass fraction
$x$	:	Direction of diffusion
$Z$	:	Number of electron per atom

## LIST OF PUBLICATIONS

1. **J. Banjuraizah**, H. Mohammad, Z. A. Ahmad. "Synthesis and characterization of  $x\text{MgO}-1.5\text{Al}_2\text{O}_3-5\text{SiO}_2$  ( $x = 2.6 - 3.0$ ) system using mainly talc and kaolin through the glass route" **Materials Chemistry and Physics**, *Accepted 13 May 2011*.
2. **J. Banjuraizah**, H. Mohammad, Z. A. Ahmad. "Effect of impurities content from minerals on phase transformation, densification and crystallization of  $\alpha$ -cordierite glass-ceramic" *Journal of Alloys and Compounds*, Article in Press doi:10.1016/j.jallcom.2011.04.
3. **J. Banjuraizah**, H. Mohammad, Z. A. Ahmad. " Effect of excess MgO mole ratio in stoichiometric cordierite ( $2\text{MgO}.2\text{Al}_2\text{O}_3.5\text{SiO}_2$ ) composition on phase transformation and crystallization behavior of magnesium aluminum silicate phases". *International Journal of Applied Ceramic Technology*. Volume 8, Issue 3, May 2011, Pages 637-645
4. **J. Banjuraizah**, H. Mohammad, Z. A. Ahmad "Densification and crystallization of non stoichiometric cordierite compositions with excess MgO mole ratio syntheses from kaolin and talc" *Journal of American Ceramic Society*. Volume 94, issue 3, March 2011. Pages 687-694
5. **J. Banjuraizah**, H. Mohammad, Z. A. "Effect of melting temperatures on the crystallization and densification of  $2.8\text{MgO}.1.5\text{Al}_2\text{O}_3.5\text{SiO}_2$  glass-ceramic synthesized from mainly talc and kaolin". *Journal of the Alloys and Compound*, Volume 509, Issue 5, 3 February 2011, Pages 1874-1879 (2010)
6. **J. Banjuraizah**, H. Mohammad, Z. A. Ahmad. "Thermal expansion coefficient and dielectric properties of non-stoichiometric cordierite compositions with excess MgO mole ratio synthesised from mainly kaolin and talc by the glass crystallization method. *Journal of Alloys and Compounds*. Volume 494, January 2010. Pages 256-260
7. **J. Banjuraizah**, H. Mohammad, Z. A. Ahmad. "Crystal Structure Of Single Phase And Low Sintering Temperature Of  $\alpha$ -Cordierite Synthesized From Talc And Kaolin". *Journal of Alloys and Compounds*, Volume 482, Issues 1-2, 12 August 2009, Pages 429-436.

8. **J. Banjuraizah**, H. Mohammad, Z. A. Ahmad "Rietveld Quantitative Phase Analysis Of Non-Stoichiometric Cordierite Synthesized From Mainly Talc And Kaolin: Effect Of Sintering Temperature" *Journal of Nuclear and Related Technologies (JNRT)* 2009. Volume 6, No. 1 (Special Edition) 2009 ISSN 1823-0180
9. **J. Banjuraizah**, H. Mohammad, Z. A. Ahmad "Characterization Of Cordierite Based Glass Synthesis From Pure Oxide And Minerals" *Journal of Nuclear and Related Technologies (JNRT)* 2009. Volume 6, No. 1 (Special Edition) 2009 ISSN 1823-0180
10. **J. Banjuraizah**, M. N. Derman, H. Mohammad, Z. A. Ahmad. "Effect of excess MgO molar ratio in Crystallization and Phase Evolution of cordierite synthesized by crystallization of glass method using talc and kaolin" **International Graduate Conference on Engineering and Science (IGCES 2008)**. Universiti Teknologi Malaysia, Skudai, Johor Bahru, 23 - 24 December 2008.
11. **J. Banjuraizah**, H. Mohammad, Z. A. Ahmad " Comparative study on cordierite based glass synthesis from pure oxide and abandon materials" **The 4<sup>th</sup> International Conference on X-Rays and Related Techniques in Research and Industries 2008 (ICXRI 2008)**. Universiti Malaysia Sabah, Kota Kinabalu, Sabah. 2-6 Jun 2008.
12. **J. Banjuraizah**, H. Mohammad, Z. A. Ahmad "Rietveld Quantitative Phase Analysis of Cordierite Based Glass". *The 4<sup>th</sup> International Conference on X-Rays and Related Techniques in Research and Industries 2008 (ICXRI 2008)*. Universiti Malaysia Sabah, Kota Kinabalu, Sabah. 2-6 Jun 2008.
13. **J. Banjuraizah**, H. Mohammad, Z. A. Ahmad. "Crystal structure analysis and estimating crystallite size of  $\alpha$ -cordierite synthesized from different MgO-Al<sub>2</sub>O<sub>3</sub>-SiO<sub>2</sub> ratio using various Fundamental Parameter Approach" **Nanomaterials Synthesize and Characterization Conference'** Palace of Golden Horses, Seri Kembangan (nMSC2009). 3-4 November 2009.
14. **J. Banjuraizah**, H. Mohammad, Z. A. Ahmad. "Effect of mechanical activation parameter to degree of contamination and particle size of cordierite glass powder" **Nanomaterials Synthesize and Characterization Conference'** Palace of Golden Horses, Seri Kembangan (nMSC2009). 3-4 November 2009.

# SINTESIS KORDIRIT TAK STOIKIOMETRIK MELALUI KAEDAH KACA-SERAMIK MENGGUNAKAN TALKUM DAN KAOLIN TERKALSIN

## ABSTRAK

Pelbagai komposisi tak stoikiometrik kordirit telah disintesis melalui kaedah penghabluran kaca. Kelakuan pepadatan dan penghabluran kaca ditentukan menggunakan ujian dilatometri, dan analisis pembezaan terma. Manakala transformasi fasa kaca ke kaca-seramik menggunakan pembelauan sinar-x. ujian pekali pengembangan terma, sifat dielektik, ketumpatan dan peratus porositi serta mikrostruktur kaca-seramik dilakukan untuk mengaitkan perubahannya terhadap komposisi. 100 wt% fasa hablur  $\alpha$ -kordierit dengan ketumpatan  $2.54 \text{ g/cm}^3$ , porositi 0.4 % telah berjaya diperolehi pada suhu rawatan haba serendah  $900^\circ\text{C}$  selama 2 jam menggunakan komposisi tak stoikiometrik kordirit yang di sintesis menggunakan talkum dan kaolin terkalsin sebagai bahan mula. Ini menunjukkan komposisi ini sesuai untuk aplikasi LTCC. Pekali pengembangan terma ( $2 \times 10^{-6} \text{ C}^{-1}$ ), pemalar dielektrik (5.5) and kehilangan dielektrik ( $1.6 \times 10^{-2}$ ) yang diperolehi juga memenuhi sifat-sifat yang diperlukan untuk aplikasi frekuensi tinggi. Fasa separuh amorfus pada serbuk kaca mula perlu dielakkan kerana ia akan memberikan kesan yang besar pada kelakuan pepadatan dan penghabluran kaca.  $\alpha$ -kordierit yang di sintesis dari mineral sebagai bahan mula mempunyai sifat-sifat yang standing dengan  $\alpha$ -kordierit yang dihasilkan dari oksida tulen. Namun, ia mempunyai darjah penghabluran yang rendah dan mempunyai kehilangan dielektik yang tinggi berbanding sampel yang disintesis menggunakan oksida tulen. Penambahan  $\text{B}_2\text{O}_3$  and  $\text{P}_2\text{O}_5$  sangat berkesan dalam menurunkan suhu pelembutan tetapi tidak semestinya meningkatkan proses penghabluran. Ia hanya berkesan pada sampel-sampel dalam siri  $x\text{MgO}.2\text{Al}_2\text{O}_3.5\text{SiO}_2$  yang mempunyai bilangan mol MgO yang rendah. Adalah sangat penting untuk melebur campuran komponen di atas suhu peleburan sebelum penghabluran kerana sistem kaca + kaca-seramik dalam system yang sama tidak dapat meningkatkan pepadatan disebabkan oleh halangan kinetik yang tinggi di antara sistem.

## THE SYNTHESIS OF NON-STOICHIOMETRIC CORDIERITE VIA GLASS CERAMIC ROUTE USING CALCINED TALC AND KAOLIN

### ABSTRACT

Various non-stoichiometric cordierite compositions were synthesized via glass route. Densification and crystallization behavior of the glass were determined by dilatometry and differential thermal analysis, while phase transformation of glass to glass-ceramic by X-ray diffraction. CTE, dielectric properties, density and porosity percentages as well as the microstructure of glass-ceramic were carried out to correlate its variation with the compositions. 100 wt%  $\alpha$ -cordierite phase with the density 2.54 g/cm<sup>3</sup>, porosity 0.4% has successfully being obtained at lower heat treatment temperature of 900°C for 2 hours using non-stoichiometric cordierite compositions synthesized from mainly calcined talc and kaolin as initial raw materials. This demonstrates that this composition is suitable for LTCC application. The CTE ( $2 \times 10^{-6} \text{ C}^{-1}$ ), dielectric constant (5.5) and dielectric loss ( $1.6 \times 10^{-2}$ ) obtained are also fulfilled the properties required for high frequency application. Partially amorphous phase in initial glass powder should be avoided since it will significantly affect the densification and crystallization behavior of the glass.  $\alpha$ -cordierite synthesized from minerals as raw materials has a comparable properties with the one synthesized reagent grade oxide. Although it has slightly lower degree of crystallinity and high dielectric loss, however it has lower densification and crystallization temperature as compared to composition synthesized from the reagent grade oxides. The addition B<sub>2</sub>O<sub>3</sub> and P<sub>2</sub>O<sub>5</sub> are effective in reducing the softening temperature but not necessarily enhance the crystallization process. The addition of B<sub>2</sub>O<sub>3</sub> and P<sub>2</sub>O<sub>5</sub> is only effective for samples in the series xMgO.2Al<sub>2</sub>O<sub>3</sub>.5SiO<sub>2</sub> with lower MgO mole. It is also a very important to melt the mixtures of compounds above its melting point before crystallize since glass plus glass-ceramic in the same system would not facilitate densification due to its relatively high kinetic barrier within the system.

# CHAPTER 1

## INTRODUCTION

### 1.1 Introduction

Recently, high circuit density packages for miniaturization and for lightweight integrated electronic assembly are required in wireless communication and high frequency applications [1, 2]. Therefore, several researches on compact multilayer structures with buried passive components has gain an interest among the reseachers [3, 4]. The use of multilayer substrate decreased the time it takes for the signal to be transmitted. Hence, material with low dielectric constant is required by semiconductor industry to meet the challenge of improving integrated circuit speed by reducing the capacitance and crosstalk between metal-to-metal interconnections [5]. In addition, the thermal coefficient of the materials should also be closely matched with the chips material which is usually silicon. If the expansions were not closely matched, then the reliability of the package is reduced. If the mismatch is large enough, there will be stresses on the solder part and between the chip and the substrate. These can lead to cracking of the pads and results in open circuit and chip detachment from the substrate, which finally leads to a catastrophic failure.

Many researches have been done on multilayer structure e.g. low temperature cofired ceramic, LTCC materials and among them that have been proposed as one of the most suitable materials is cordierite since it has low dielectric constant ( $\epsilon = 5-6$ ), high resistivity ( $\rho > 10^{12} \Omega\text{cm}$ ), elevated thermal and chemical stabilities, very low coefficient of thermal expansion, CTE ( $\alpha=1-2 \times 10^{-6} \text{ C}^{-1}$ ), and excellent insulation properties [6]. These are the properties of high purity and crystallinity of  $\alpha$ -cordierite

phase which normally can be obtained by sintering cordierite initial powders at temperature above 1200°C [7-9]. Although  $\alpha$ -cordierite is a promising material for high speed application due to its low dielectric constant, low dissipation factor and low thermal expansion, but it is difficult to crystallize and sinter  $\alpha$ -cordierite phase below 1000°C because of its sintering temperature range (1200-1350°C) [10-13] is near to the incongruent melting point of the cordierite. It has the incongruent melting point because the solid compound of cordierite does not melt to form the liquid of its composition, but instead dissociates to form a new solid phase and the liquid. The lowest liquidus temperature is at the tridymite- protoenstatite-cordierite eutectic at 1345°C, and cordierite-enstatite-forsterite at 1360°C [14]. Many researches have been conducted in order to find out how to decrease the sintering temperature of cordierite. Some of them have used flux or additives whilst others have tried to synthesize it using different method such as sol-gel process, non hydrolytic sol-gel process and cordierite glass powder. Among those techniques, glass-ceramic route has successfully obtained  $\alpha$ -cordierite at and below 1000°C [15-21]. The sintering temperature of the dielectric materials has to be reduced  $\leq 900^\circ\text{C}$  [22, 23] in order to allow metal pastes with high electrical conductivity e.g. Ag, Au, and Cu. This is because of the sintering temperature of Ag, Au or Cu electrodes (the melting point of Ag: 961.93°C, Au: 1064.43 °C, Cu: 1083°C) in multilayer device has limit the sintering temperature of the substrate to 0.7 of its melting point ( $0.7T_m$ ). Therefore, all glass powders with various compositions in the present study were characterized after subjected to 900°C heat treatment temperature.

It is not enough to crystallize  $\alpha$ -cordierite below 1000°C by only applying crystallization of glass method. Normally various nucleating agent or sintering aids were also used. Although some of these authors have successfully crystallized  $\alpha$ -cordierite to below 1000°C by the addition of additives, however other secondary phases were also present and as a result it will degrade some of the required properties. By using cordierite composition with additives, Chen et al. [21] and Wang et al. [18] had successfully synthesized  $\alpha$ -cordierite below 1000°C. However, Chen et al. [20, 21] found that although the increasing of CaO or ZnO content could decrease the crystallization temperature of  $\alpha$ -cordierite and increased the peak intensity of  $\alpha$ -cordierite but other phase which are gahnite and mullite [20] are also present which finally increase the coefficient of thermal expansion CTE of samples. Wang et al. had used less than 5 wt %,  $B_2O_3$  and  $P_2O_5$  and only small amount of  $\alpha$ -cordierite was found to crystallize at 850°C, and a single phase of  $\alpha$ -cordierite was only obtained at 1050°C [18].

In magnesium aluminum silicate (MAS) glass system, MgO is a modifying oxide,  $Al_2O_3$  is an intermediate oxide and  $SiO_2$  is a glass former [24]. Modification on the ratio of MAS system would be beneficial to lower the viscosity of the glass and enhance the nucleation rate. It was reported in the literature reviews [20, 21, 25-27] using pure oxide as initial raw materials that cordierite composition with excess MgO and less  $Al_2O_3$  would also contribute to better densification and crystallization behavior. Since an excess of MgO from stoichiometric cordierite composition could retard the formation of  $\mu$ -cordierite, enhanced the densification and crystallization



behavior of  $\alpha$ -cordierite phase, a few series of non-stoichiometric cordierite compositions were studied in the initial stage without any additives using mainly talc and kaolin, and crystallization by the glass route has been selected as method of synthesis.

There were various types and mixtures of raw materials have been used to synthesize  $\alpha$ -cordierite. Talc and kaolin which contain high amount of MgO, Al<sub>2</sub>O<sub>3</sub> and SiO<sub>2</sub> have also been used as the initial raw materials for synthesizing  $\alpha$ -cordierite. Even though, there are many studies on the synthesized of  $\alpha$ -cordierite using talc and kaolin as the starting raw materials together with other minerals such as magnesium compounds [39], silica, alumina [40], gibbsite [31,41], calcined alumina and fly ash [32], magnesium oxide [42], diatomite and alumina [36], silica, sepiolite and feldspar [43], fly ash, fused silica and alumina mixture [33], alumina [44,45]; however, most of them followed solid state reaction route except two [1,10] used glass crystallization method. The presence of secondary phases on sintered samples previously reported using these minerals, together with the existence of impurities content in the minerals may be the reasons of limited researches found on crystallization of  $\alpha$ -cordierite from minerals by glass-ceramic route especially for electronic packaging application. Conversely, talc and kaolin contain alkali oxides and alkaline earth oxides which may facilitate in decreasing the melting temperature as well as its densification and crystallization temperature of glass-ceramic.

For that reason, in this present study talc and kaolin were selected as the main initial raw materials for synthesizing  $\alpha$ -cordierite, while small amount of MgO,

$\text{Al}_2\text{O}_3$ ,  $\text{SiO}_2$  were added just to compensate the chemical formulation. Comprehensive investigation on the glass-ceramic between two groups of samples from different initial raw materials namely pure oxides and minerals with the same  $\text{MgO}:\text{Al}_2\text{O}_3:\text{SiO}_2$  (MAS) ratios and similar processing parameters is essential to provide an understanding on how the impurities affect the properties of glass-ceramic. Therefore, a few samples of the same formulations were produced from pure oxide for detail observation on the trend of phase transition, densification and crystallization of samples and then, make a comprehensive comparison with samples produced using mainly talc and kaolin as initial raw materials.

The combination of  $\text{P}_2\text{O}_5$  and  $\text{B}_2\text{O}_3$  are commonly used in crystallization of  $\alpha$ -cordierite from glass [18, 21, 28-33]. Although the addition of  $\text{B}_2\text{O}_3$  and  $\text{P}_2\text{O}_5$  is effective to enhance the densification and crystallization of  $\alpha$ -cordierite phase, however, the final glass-ceramic properties would deteriorate if too much nucleating agent were added in the compositions. Therefore, the effect of the addition of 3 wt%  $\text{B}_2\text{O}_3$  and 2 wt%  $\text{P}_2\text{O}_5$  in selected non-stoichiometric samples were examined in the present study.

Apart from that, others parameters could also affect the final properties of cordierite. Hing et al. [34] studied on the effect of processing parameters on the sinterability, microstructures and dielectric properties of glass ceramics in the cordierite phase field. They found that the nature of the precursors have a very marked effect on the densification, microstructures and dielectric properties of the sintered components. For example, mechanical milling caused surface area,

activation energy, and particle size of the initial raw materials to change. Many atoms and ions are at the surface with finer particles, and as a result, a collection of fine particles of a certain mass has higher energy than for a solid cohesive material of the same mass [35]. High surface area and accumulated energy produced has caused the reaction between particles easily occurred at much lower temperature during solid state reaction. The changes in surface area, particle size and distribution of particle size have a direct influence on the final properties. This is because final properties of end product depend on structure, mass transport and reactivity. A study had proven that the sintering temperature of certain materials could be lowered by a modification of particle size, its distribution and degree of crystallinity. Even though the chemical compositions of the mixture are the same, but the accumulated energy produced during mechanical activation give significant effect on phase transformation during sintering. It was proven that mechanical milling can caused the loss of crystalline structure of the initial powder and the increase in reactivity [36]. Yalamac et al. [37] who have conducted research on intensive grinding effect on cordierite synthesis by solid state reaction using kaolin, talc and  $\text{Al}(\text{OH})_3$  as precursor found that, by mechanical activation (maximum speed 500 rpm and maximum milling time 60 min) cordierite can be crystallized at  $1100^\circ\text{C}$  instead of above  $1200^\circ\text{C}$  [7-9] by using solid state reaction process. Furthermore, they found that a combination of additives and mechanical activation of the powder could lower the synthesis temperature of  $\alpha$ -cordierite phase at  $1000^\circ\text{C}$ . Therefore, frits that were obtained from all compositions were subjected to high energy milling using planetary mill with tungsten carbide as its grinding media. Frits were pulverized to a very fine glass powder with average particles size of 1-3  $\mu\text{m}$ .

In this study  $\alpha$ -cordierite sample was prepared in the form of bulk sample. Investigation on phase transformation, densification and crystallization behavior of glass to glass-ceramic is important to determine which compositions could produce dense, high purity and high crystalline of  $\alpha$ -cordierite phase at lower crystallization heat treatment temperature (900°C). Therefore, to determine this, dilatometry test of unsintered glass powder, isothermal and non-isothermal DTA, XRD analysis of glass powder and sintered pellet were carried out. Beside the densification and crystallization temperature, the purity and degree of crystallinity of  $\alpha$ -cordierite phase will also determine the best selection of composition used for synthesizing  $\alpha$ -cordierite phase. Rietveld method was employed for quantitative phase analysis while Full Profile method for measuring the crystallinity of  $\alpha$ -cordierite phase. Microstructure of the fractured surface, its density and porosity tests will be used to support the results. Meanwhile the results of CTE and dielectric test would confirm the physical characteristic of the samples in order for it to be used as a material for high frequency applications.

## **1.2 Problem statement**

Single phase or pure  $\alpha$ -cordierite with high degree of crystallinity had been produced by previous researchers which is suitable to be used for LTCC or substrate for high frequency application. However that particular  $\alpha$ -cordierite was obtained at higher temperature of above 1200°C. In order for it to be used for that application,  $\alpha$ -cordierite phase has to be synthesized around 900°C. Only a few researches, have successfully crystallized  $\alpha$ -cordierite from glass route below 1000°C after using pure

oxides as precursors with non-stoichiometric cordierite composition together with the addition of sintering aids or nucleating agent. However, small amount of secondary phases were still present. Thus, investigation on non-stoichiometric compositions in MAS system is necessary to obtain high purity and high degree of crystallinity of  $\alpha$ -cordierite phase. The use of pure oxide is more costly compared to the use of talc and kaolin as initial raw materials. Furthermore, the minerals used in the present study contain alkali oxides and alkaline earth oxides elements which could act as fluxes. Therefore, with appropriate composition design, there is a possibility to decrease the melting and crystallization temperature using these minerals.

### 1.3 Research objectives

This study is mainly concentrating on the characterization of various stoichiometric and non-stoichiometric cordierite compositions by crystallization of glass method using mainly talc and kaolin as initial precursors to obtain highest purity and crystallinity of  $\alpha$ -cordierite phase at lower sintering temperature (900°C). Therefore, the main objectives are:

- i. To synthesize and study on the densification, crystallization and properties of various cordierite phase from mainly talc and kaolin without the addition of sintering aids: a)  $x\text{MgO}.2\text{Al}_2\text{O}_3.5\text{SiO}_2$ , when  $x = 2.0$  to  $4$ , and b)  $x\text{MgO}.1.5\text{Al}_2\text{O}_3.5\text{SiO}_2$  when  $x = 2.6$  to  $3.0$ .
- ii. To investigate the effect of the addition of fixed amount of sintering aids (3 wt%  $\text{B}_2\text{O}_3$  and 2 wt%  $\text{P}_2\text{O}_5$ ) in selected stoichiometric formulations on their densification, crystallization and end properties of crystallized glass.

- iii. To compare densification, crystallization and properties of selected stoichiometric cordierite synthesized from pure oxides with the one synthesized using mainly talc and kaolin.
- iv. To observe the effect of melting temperature to densification and crystallization of glass and glass-ceramic produce from mainly talc and kaolin as the raw materials.

#### **1.4 Scope of research**

- i. In general, this study is divided into 7 Parts. Characterization of material are carried out in Part 1. Characterization of glass and glass-ceramic from non-stoichiometric cordierite composition are carried out in Part 2. In this part, the effect of varying MgO mole from the exact stoichiometric was studied. Based on the results obtained from Part 2, a series of samples with excess MgO and less  $\text{Al}_2\text{O}_3$  were produced and characterized in Part 3 to further retard the formation of secondary phase. Upon completion of Part 2 and Part 3, a few MAS composition from the above series was selected. The effect of the addition of small and fixed amount of sintering aid was examined in Part 4. The sintering aids were mixed with glass-ceramic precursors in ball milling and were subjected to similar processing parameters as the previous one. In Part 5, selected MAS composition was reproduced using pure oxides as initial raw materials to observe the trend of phase transition, densification and crystallization of glass as a function of MgO mole. The best composition from pure oxides and minerals were selected and a detailed comparison will be reported in Part 6 on whether the

characteristic of  $\alpha$ -cordierite synthesized using mainly talc and kaolin could be as good as the one synthesized using pure oxides. In order to further reduce the cost of melting, effect of melting temperature was studied in Part 7.

- ii. A study on phase transformation of glass from amorphous phase to crystalline state was studied using X-ray diffraction of fine glass powder. Qualitative and quantitative analysis were carried out using HighScore Plus software. Phase content, lattice change, crystallite size, degree of crystallinity and crystal structure analysis of samples were revealed by Rietveld method.
- iii. A non-isothermal dilatometry test was carried out on green body samples to observe the sintering reaction and shrinkage of sample at elevated temperature. From the shrinkage curve, the softening temperature or temperature at which the densification process obviously started and stopped was estimated. Activation energy for densification was also measured from dilatometry curve using Arrhenius equation.
- iv. Crystallization behavior was studied by isothermal and non-isothermal DTA analysis of all glass powder samples to determine temperature range of crystallization. From the dilatometry and DTA analyses, conclusion can be made as to which compositions have low densification and crystallization temperature. Furthermore, temperature difference between the temperature at which densification has almost completed and the temperature at which crystallization started, as well as its total percentage of shrinkage during sintering will determine the extent of how good the densification of samples.

- v. The effect of phase transition, densification and crystallization of glass as a function of variable parameters (compositions, melting temperature, sintering aids) would vary the properties of materials e.g. the CTE and dielectric properties of the sintered samples. Therefore, these properties were measured using dilatometer model Linseis and impedance analyzer (Hewlett Packard model HP4291) in order to identify its changes towards variable parameters, and consequently outline which compositions are close to the required properties for high frequency application (dielectric constant as low as possible ( $\sim 5$ ), low CTE which is close to Si chips  $-(3-3.5 \times 10^{-6}/\text{C})$  [21].
- vi. Density, porosity, and the microstructure analyses of sintered pellets were examined to support the discussions on the densification of samples



## **CHAPTER 2 LITERATURE REVIEW**

### **2.1 $\alpha$ -Cordierite**

Indialite, high cordierite or hexagonal cordierite are the terms that are sometime being used to name  $\alpha$ -cordierite. The stoichiometric formula of  $\alpha$ -cordierite is  $2\text{MgO}\cdot 2\text{Al}_2\text{O}_3\cdot 5\text{SiO}_2$ .  $\alpha$ -cordierite is one of the polymorph in cordierite system. Its density is  $2.512\text{ g/cm}^3$  and has high melting temperature which is  $1460^\circ\text{C}$ ) [14].

$\alpha$ -cordierite has been extensively studied due to their excellent properties e.g. low thermal coefficient, low dielectric constant, excellent thermal shock resistance, as well as high chemical and thermal stability. The application and potential of  $\alpha$ -cordierite materials cover a wide range of fields such as refractories, electrical, insulator, filters, membranes, heating elements, microwave absorbants, multilayer chip inductor [18], electromagnetic wave absorbants [38], honeycomb catalytic support for automobiles [39, 40] and low temperature cofired ceramic (LTCC) [5, 21, 41] .

### **2.2 MgO-Al<sub>2</sub>O<sub>3</sub>-SiO<sub>2</sub> phase**

In order to understand the crystallization behavior of cordierite precursor on heating, equilibrium phase diagrams of the MgO-Al<sub>2</sub>O<sub>3</sub>-SiO<sub>2</sub> system are needed. All primary phases obtained from these phase diagrams provide useful information to

further predict the secondary phases in the MgO-Al<sub>2</sub>O<sub>3</sub>-SiO<sub>2</sub> system. Figure 2.1 shows the ternary phase diagram of MgO-Al<sub>2</sub>O<sub>3</sub>-SiO<sub>2</sub> system. Beside cordierite, other phases such as forsterite, spinel, sapphirine, enstatite, cristobalite, tridymite, mullite, periclase, and corundum may exist in MAS system, and it's greatly depended on the MAS compositions and the sintering temperatures.

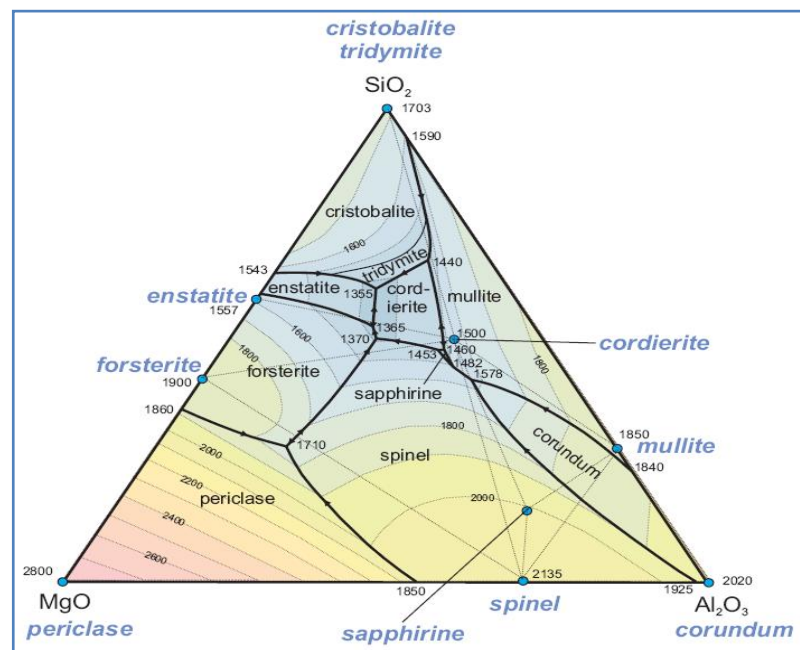


Figure 2.1 Ternary phase diagram of MgO-Al<sub>2</sub>O<sub>3</sub>-SiO<sub>2</sub> [42]

### 2.3 Polymorphism of cordierite

Cordierite exist under three polymorphic forms: i) hexagonal cordierite, high cordierite, indialite or  $\alpha$ -cordierite with a space group P6/mmc, ii) orthorhombic or  $\beta$ -cordierite with a space group Cccm, and iii) meta-stable form referred to  $\mu$ -cordierite or magnesium aluminum silicate with a space group P6222/160.  $\mu$ -cordierite is a solid solution with  $\beta$ -quartz structure [43]. Both  $\mu$ -cordierite and  $\beta$ -

quartz has the same space group with slightly similar diffraction pattern and similar arrangement of atoms in the crystal as shown in Figure 2.2. In  $\mu$ -cordierite the  $Mg^{+2}$  cation occupying octahedral sites between the two tetrahedral sites.

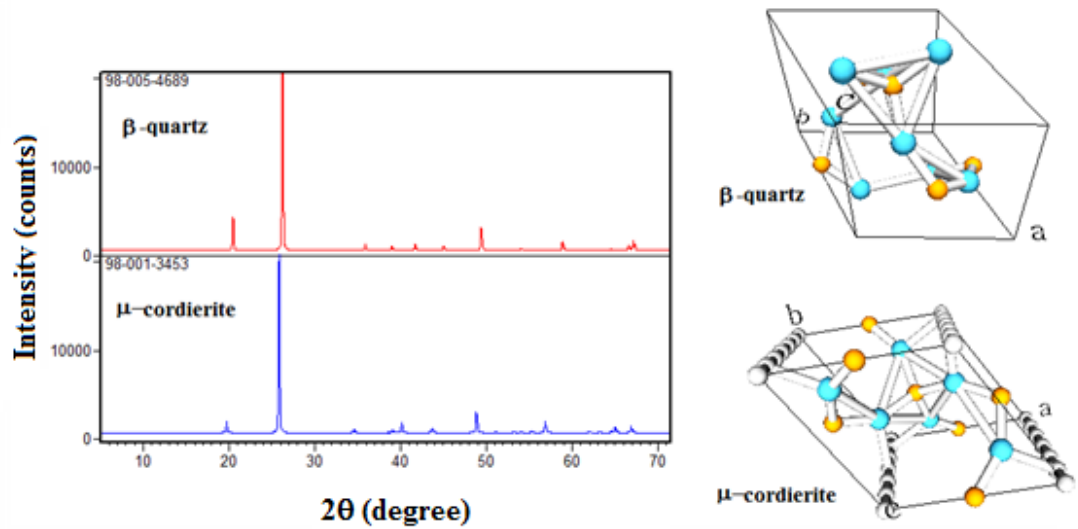


Figure 2.2 Diffraction pattern and crystal structure plots of  $\mu$ -cordierite and  $\beta$ -quartz

The crystal structure plots for the three polymorphs are shown in Figure 2.3 to Figure 2.5. Table 2.1 shows crystal structure data of the three cordierite polymorphs.

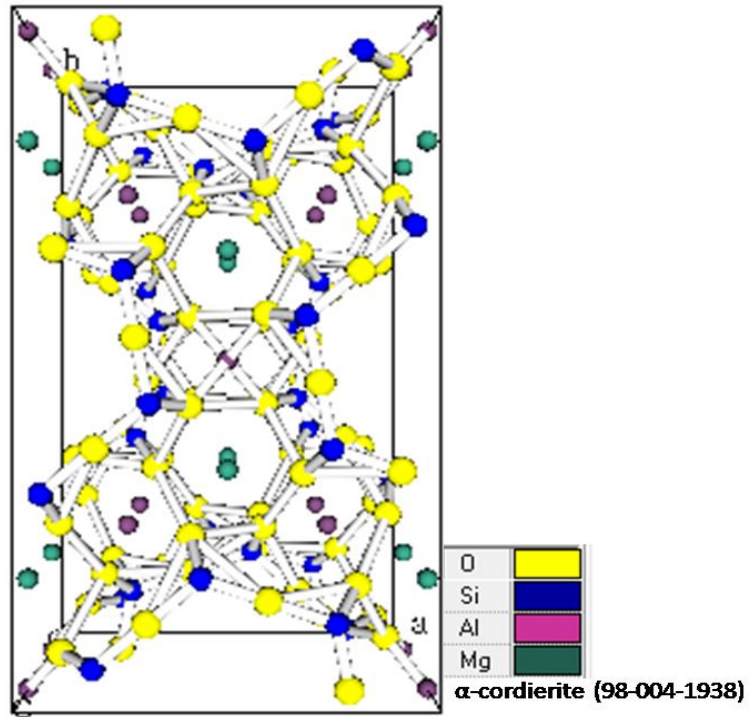


Figure 2.3 Crystal structure of  $\alpha$ -cordierite (ICSD 98-004-1938)

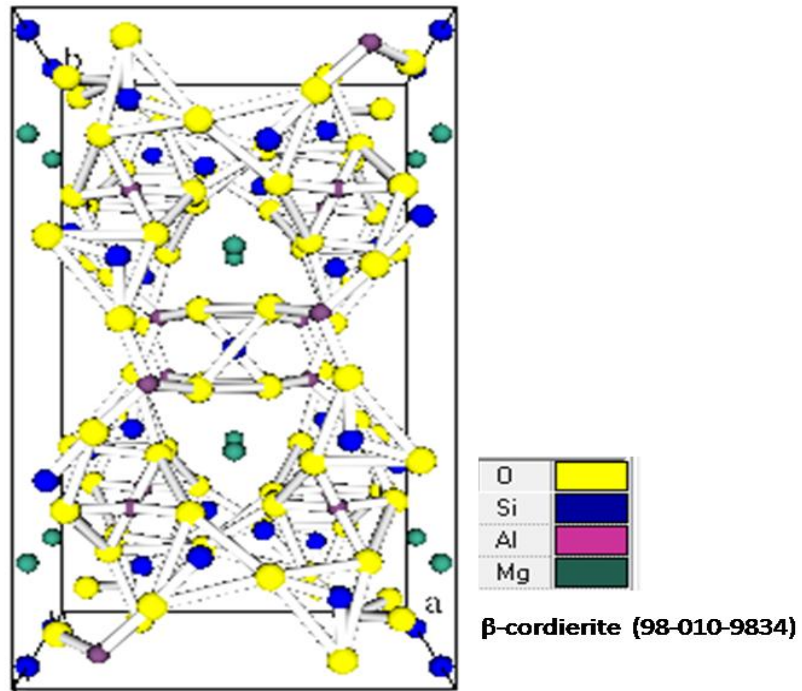


Figure 2.4 Crystal structure of  $\beta$ -cordierite (ICSD 98-010-9834)

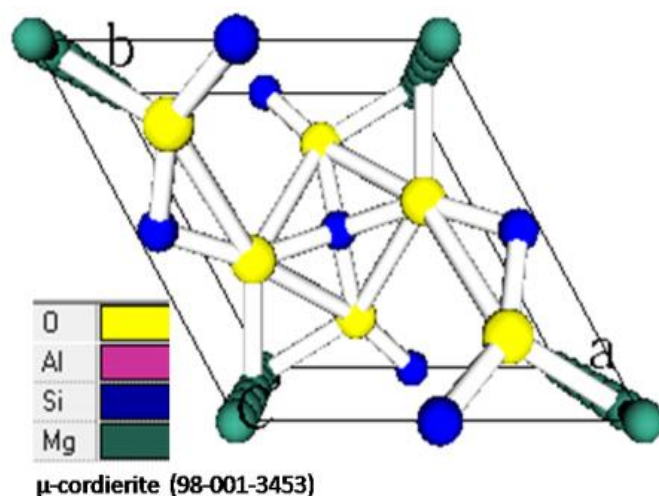


Figure 2.5 Crystal structure of  $\mu$ -cordierite (ICSD 98-001-3453)

Table 2.1 Crystal data for  $\mu$ -cordierite,  $\alpha$ -cordierite and  $\beta$ -cordierite taken from Inorganic Crystal Structure Database (ICSD)

Property	$\mu$ -Cordierite	$\alpha$ -Cordierite or high cordierite	$\beta$ -Cordierite or low cordierite
Crystal system	Hexagonal ( $a=b \neq c$ )	Hexagonal ( $a=b \neq c$ )	Orthorhombic $a \neq b \neq c$
ICSD no	98-001-3453	98-004-1938	98-010-9834
Space group	P6222(160)	P6/mcc(192)	Cccm (66)
Lattice $a$	5.182	9.768	9.647
Lattice $b$	5.182	9.768	16.975
Lattice $c$	5.360	9.341	9.2740
Distortion index ( $\Delta$ )	n/a	0	0.24°

According to Velasco et al. cordierite have a tetrahedral silicates framework with the simplified structure formula  $Mg_2Al_4Si_5O_{18}$ . The Al and Si atoms are distributed over tetrahedral sites (T) which is three T1 and six T2 site per formula units [44]. Sai Sundar et al. described the structure of cordierite are built up layers of

corners-shared tetrahedral (S/Al)O<sub>4</sub> and octahedral [45]. There are two types of layer. First layers are the layers of (S/Al)O<sub>4</sub> tetrahedral forming hexagonal ring, and the second layers with (S/Al)O<sub>4</sub> tetrahedral intermixed with MgO<sub>6</sub>. The hexagonal and orthorhombic structures are characterized by their six-membered rings of tetrahedrally coordinated cations (T2) which was perpendicular to *c* axis. Mg atoms are located in slightly flattened octahedral. Alternate layers of the hexagonal rings structure are connected through Mg octahedral and T1 tetrahedra. Silicon occupies mostly T2 tetrahedra, and aluminum T1 tetrahedra. The difference between  $\alpha$ -cordierites and  $\beta$ -cordierite lies in a greater or lesser degree of disorder between the aluminum and silicon atoms within T1 and T2 sites [43]. The diffraction pattern of  $\beta$ -cordierite and  $\alpha$ -cordierite are very similar as shown in Figure 2.6.

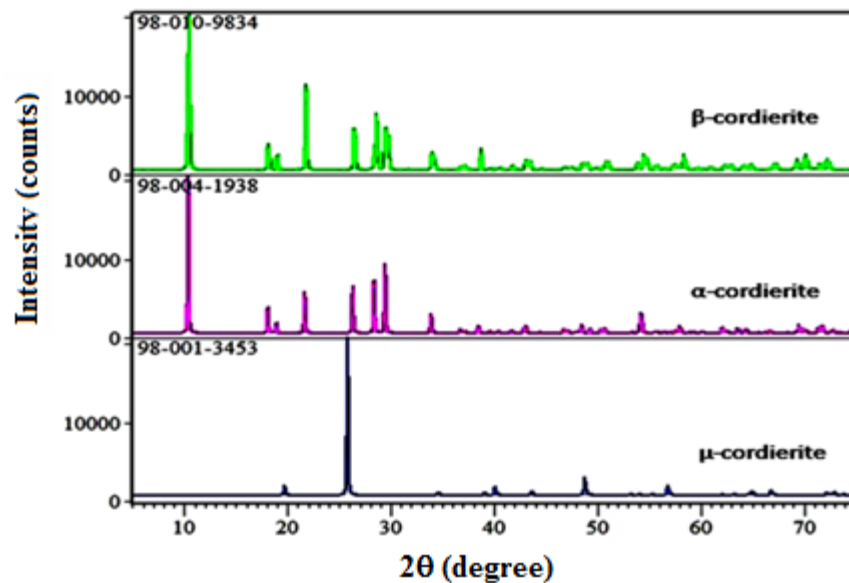


Figure 2.6 Reference pattern of 3 cordierite polymorphs  $\alpha$ -cordierite,  $\beta$ -cordierite,  $\mu$ -cordierite

Both  $\alpha$ -cordierite and  $\beta$ -cordierite polymorphs can be distinguished by evaluating the  $2\theta$  range from  $28^\circ$  to  $30^\circ$  as shown in Figure 2.7. In this range, one can see that  $\alpha$ -cordierite displays only 2 peaks, while cordierite displays up to 5 different peaks [44].

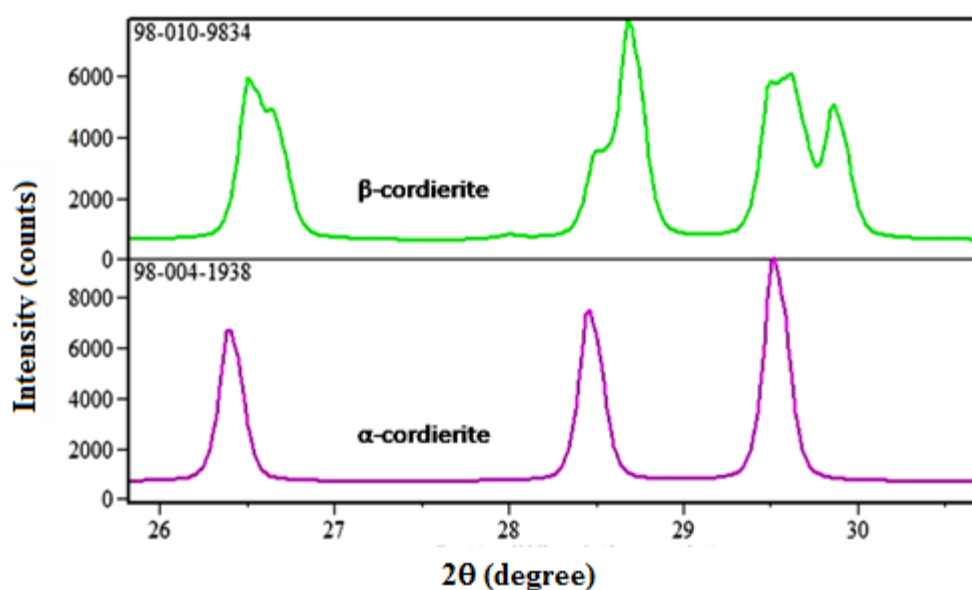


Figure 2.7 Diffraction pattern of hexagonal and orthorhombic cordierite can be distinguished after zooming at  $2\theta$  28- $30^\circ$

The identification peaks at  $29$ - $30^\circ$  of the  $2\theta$  range reveals that the line corresponding to (211) planes has been divided into three orthorhombic peaks which are assigned to (151), (241) and (311) planes, respectively. This behavior shows the transformation of the polymorph with hexagonal symmetry,  $\alpha$ -cordierite into polymorph with orthorhombic symmetry,  $\beta$ -cordierite. The polymorphic transformations between  $\alpha$ -cordierite and  $\beta$ -cordierite are related to states of order

and disorder of one Al atom and five Si atoms in the tetrahedral rings of the structure. Hence, the material can exhibit all structural intermediates between  $\alpha$ -cordierite and  $\beta$ -cordierite. Generally, Si and Al atoms are ordered in the  $\beta$ -cordierite structure and disordered in the  $\alpha$ -cordierite structure. The ordering sequence of Al-Si in  $\beta$ -cordierite is shown in Figure 2.8. Numerous studies have been carried out to establish the mechanisms by which this Si and Al reordering take place, especially in the case of magnesium cordierite in which two stable polymorphs co-exist in non-equilibrium states. Gonzalez [44] in his research, reported that the first structure formed was hexagonal cordierite then finally it turned into orthorhombic cordierite by calcinations at 1400°C. This means that the presence of specific polymorph is clearly dependent on the thermal treatment.

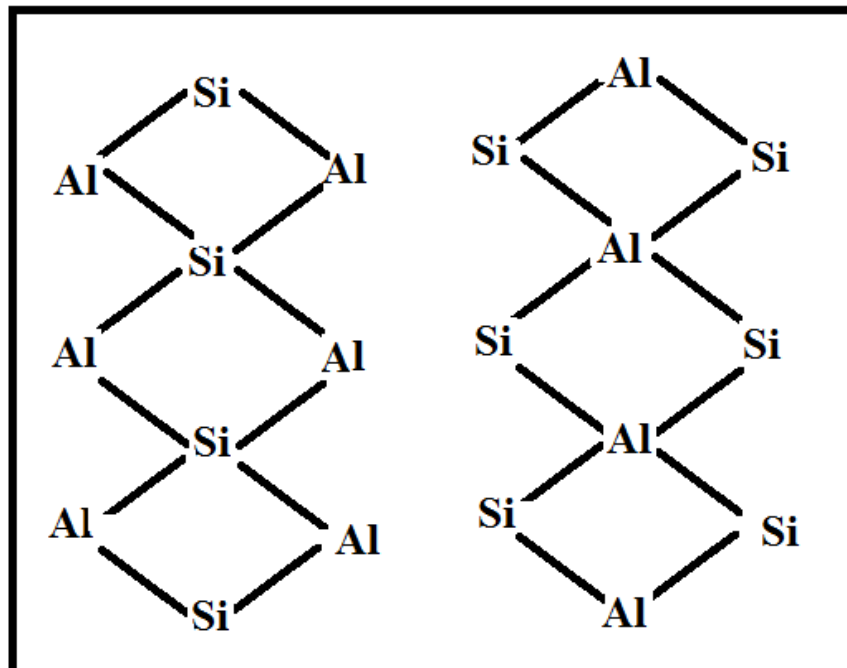


Figure 2.8 Al-Si ordering sequence in  $\beta$ -cordierite



The simplest way to determine the degree of transformation is by means of a parameter that represents the degree of distortion of the crystalline structure during its transformation from hexagonal to orthorhombic symmetry. Parameter denoted as  $\Delta$  is named as distortion index and is calculated as Equation 2.1 [44].

$$\Delta = 2\theta_{131} - \left(\frac{2\theta_{151} + 2\theta_{421}}{2}\right) \quad (\text{Equation 2.1})$$

Those phase with hexagonal crystal structure were found to be stable at the highest temperature ( $\Delta=0$ ). The orthorhombic phase corresponding to the previously named  $\beta$ -cordierite had a distortion index up to  $0.25^\circ$  and was named as low cordierite [44].

## **2.4 Common methods for synthesis of $\alpha$ -cordierite powders**

As that of other crystalline ceramic phase,  $\alpha$ -cordierite can be synthesized using various kinds of methods such as solid state reaction, sol-gel, non-hydrolytic sol-gel, hydrothermal, plasma sprayed, and crystallization of glass. However, the most common methods are by using solid state reaction, sol-gel and crystallization of glass.

### **2.4.1 Solid state reaction**

$\alpha$ -cordierite can be obtained by solid state reaction at 1200-1350°C using mixtures of starting materials (e.g. mixture of oxides, hydroxides, carbonates, kaolin, clays, talc, and chlorites) [10-13]. Grinding is necessary in order to achieve a homogeneous mixture of reactants,. The small particle sizes that are well mixed are needed in order to maximize the surface contact area. The number of particles in

contact may be increased by pelletizing the powders using a hydraulic press. Pelletizing decrease distance between particles, increase particle contact, and reduced large amounts of pore. Therefore, if enough thermal energy was supplied to the atoms or ion which exceed the energy barrier (activation energy), then the diffusion of atoms would occur, and particles are easily coalesce by material transport. Interstitials and substitutional of ions or atoms occurs during diffusion in order to achieve electroneutrality.

Sintering temperature for single phase oxides typically fall in the range of 0.75-0.90 of the melting temperature ( $T_m$ ) [46], and with a reasonable reaction time to overcome the lattice energy so that a cation can diffuse into a different site [44].

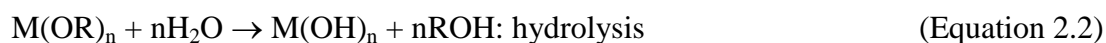
The progress of chemical change will depend on the area and defect structure of the contact areas between the reactant solids and the products when liquefaction did not occur. The progress of such chemical changes is strongly influenced by two factors: i) the contact interfacial area which is not dependent on the absolute reactant mass. For instance two large single crystals touching at a small area of interfacial contact may only yield a small amount of product compared to small mass of compacted fine powder with larger contact area, and ii) the ease of diffusion of reactants through the product layer which depends upon temperature and defect structure of the product layer. Thus, solid state reaction may vary considerably between different reactant samples, and dense  $\alpha$ -cordierite phase in solid state reaction normally obtained at temperature of 1200°C-1350°C [47-49].

## 2.4.2 Sol-gel method

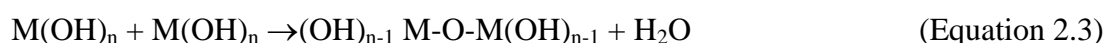
$\alpha$ -cordierite phase can also be obtained by sol-gel processes in which the components are proportionally mixed in liquid state with an organometallic precursor, producing a sol-gel system that generates the ceramic material when dried and calcined at high temperature. Sol-gel is a very attractive synthesis technique because of its ability to generate stoichiometric materials of high purity with good control over particle size. The products of the sol-gel process which having high surface area can be densified by sintering at much lower temperatures than conventional preparations.

Sol-gel techniques have been reported in the synthesis of cordierite powders using alkoxides and metal salt as the starting material[50]. In most cases tetraethylorthosilicate (TEOS) was used as a source of silicon. In general, sol-gel process involves a transition of a system from a liquid "sol" (mostly colloidal) into a solid "gel" phase. The starting materials used in the preparation of the "sol" are usually inorganic metal salts or metal organic compound such as metal alkoxides [51-53]. The sol-gel process is well known for its capability to generate oxide glasses and ceramics. The sol-gel method involves hydrolysis of metal alkoxides and subsequent condensation to yield amorphous polymeric gels. The gels can then be dried with the help of drying control additives supercritically to form xerogels, ambigels or aerogels, respectively. The dried gels when heat-treated transform to yield crystalline oxide. Metal alkoxides ( $M(OR)_n$ ) are compounds, where the metal species (M) are bound to organic carbon via oxygen [52, 54]. The alkoxy group (OR) in a metal alkoxide is a Lewis base which is an atomic or molecular species that

donates one pair electron and it undergoes hydrolysis to form a metal oxide or hydroxide as the Equation 2.2.



Polymerization and condensation



The sol-gel method can be generally utilized to generate crystalline or amorphous oxides depending on the experimental conditions such as pH in the solution, temperature and the amount of catalyst for inducing hydrolysis, etc. The sol-gel approach can provide amorphous or crystalline oxides of high purity, fine particle size and variable compositions. It has been very well exploited for synthesizing materials at lower temperature, which typically form at high temperatures using solid state reaction.

The disadvantage is due to the extreme moisture sensitivity of the alkoxide. In addition, microscopic inhomogeneity in the resultant gels and oxides due to different rates of hydrolysis for various alkoxides has been observed. Although the problem can be resolved by controlling the hydrolysis temperature, type of catalyst, concentration of alkoxides, and the amount of water. However, the process becomes more complex and is not practical for industrial applications who producing powders for bulk materials.

## **2.5 Crystallization of glass method**

Glass-ceramic materials are polycrystalline solids that are embedded in an amorphous glass matrix. It was produced by a process referred to here as “devitrification or crystallization of glass. The first step towards the transition process involves conventional techniques for glass production, followed by crystallization under carefully controlled operating conditions. These post-treatment of amorphous glass would leads to the separation of a crystalline phase from the glassy parent phase.

Glasses are formed by melting the compounds above its melting temperature followed by cooling from the liquid state at rates fast enough without crystallization. Glass-ceramics have a unique microstructure, consisting of homogeneous pore free matrix with a very fine grain, and interwoven with residual glass phase. Its properties is determined by the nature of crystalline phase, residual glass and microstructure. The composition of the parent glass and crystallization are extremely important to the final property of the glass. Glass exist in metastable state has a free energy higher than that corresponding crystalline phases of the same composition. For the purposes of attaining useful properties in a glass-ceramic, it is necessary to control the process from melting up to nucleation and growth of crystal. An understanding of nucleation and crystallization of glasses is important in order to crystallize glass with control microstructure. This is because nucleation and crystallization determine the total amount of crystalline phase devitrified from the glass upon heat treatment. Therefore, high degree of crystalline phase would be obtained if high fraction of nuclei formed and growth. Variation of nucleation and growth rate as a function of heat treatment

temperature would results in the formation of crystals with various sizes. The crystals with different size and different orientation can be observed through the size and the orientation of the grain. Meanwhile, the grain boundary of crystals demonstrates the imperfection between the crystals.

Crystallization of a glass involves the transition from the random structure of a liquid to the more ordered regular lattice of a crystalline solid. The driving force for crystallization, as with any phase transition, is by lowering the free energy of the system and in this case is by decreasing the entropy (amount of disordered). The ability of a glass to crystallize is determined by kinetic factors, and the tendency of the atoms to rearrange. Therefore, for the purpose of attaining useful property in glass, it is necessary to control the process, so that homogeneous glass can be formed easily and the glass will crystallize such that microstructure can be control by crystallization condition.

### **2.5.1 Crystallization process**

The crystallization process consists of two major events, nucleation and crystal growth. Nucleation and crystal growth are necessary in order to transform the glass from the metastable state to stable state. Thus, understanding on nucleation and growth is important since the development of crystal would not occur without the presence of nuclei.